

Broad angular anisotropy of multiple scattering in a Si crystal

A. Mazzolari¹, A. Sytov^{a,1,2}, L. Bandiera¹, G. Germogli^{1,2}, M. Romagnoni^{1,2}, E. Bagli¹, V. Guidi^{1,2}, V. V. Tikhomirov³, D. De Salvador^{4,5}, S. Carturan^{4,5}, C. Durigello^{4,5}, G. Maggioni^{4,5}, M. Campostrini⁵, A. Berra^{6,7}, V. Mascagna^{6,7}, M. Prest^{6,7}, E. Vallazza⁷, W. Lauth⁸, P. Klag⁸, M. Tamisari^{1,9}

¹INFN Sezione di Ferrara, Via Saragat 1, 44124 Ferrara, Italy

²Dipartimento di Fisica e Scienze della Terra, Università di Ferrara, Via Saragat 1, 44124 Ferrara, Italy

³Institute for Nuclear Problems, Belarusian State University, Bobruiskaya 11, Minsk 220030, Belarus

⁴Dipartimento di Fisica, Università di Padova, Via Marzolo 8, 35131 Padova, Italy

⁵INFN Laboratori Nazionali di Legnaro, Viale dell'Università 2, 35020 Legnaro, Italy

⁶INFN Sezione di Milano Bicocca, Piazza della Scienza 3, 20126 Milano, Italy

⁷Università dell'Insubria, via Valleggio 11, 22100 Como, Italy

⁸Institut für Kernphysik der Universität Mainz, 55099 Mainz, Germany

⁹Dipartimento di Scienze Biomediche e Chirurgico specialistiche, Università di Ferrara, Via Luigi Borsari 46, 44121 Ferrara, Italy

Received: date / Accepted: date

Abstract We observed reduction of multiple Coulomb scattering of 855 MeV electrons within a Si crystalline plate w.r.t. an amorphous plate with the same mass thickness. The reduction owed to complete or partial suppression of the coherent part of multiple scattering in a crystal vs crystal orientation with the beam. Experimental data were collected at Mainz Mikrotron and critically compared to theoretical predictions and Monte Carlo simulations. Our results highlighted maximal 7 % reduction of the r.m.s. scattering angle at certain beam alignment with the [100] crystal axes. However, partial reduction was recorded over a wide range of alignment of the electron beam with the crystal up to 15 deg. This evidence may be relevant to refine the modelling of multiple scattering in crystals for currently used software, which is interesting for detectors in nuclear, medical, high energy physics.

Keywords Multiple scattering · Crystal · Coherent effects

1 Introduction

Interaction of a charged particle traversing an amorphous medium occurs through repeated interactions with atoms, i.e. the so-called multiple Coulomb scattering [1, 2, 3]. This effect is essential for describing any physical

experiment connected with the passage of charged particles through matter.

A large variety of detectors, in particular semiconductor detectors, electromagnetic calorimeters, etc. require simulations of multiple scattering using special well-verified software like GEANT 4 [4], FLUKA [5] and other codes for event reconstruction. Although the materials which the detectors are frequently made of have a crystalline structure, they are usually treated with a multiple scattering model for an amorphous media. Since a crystal is a solid material whose constituents, such as atoms, molecules or ions, are arranged in a periodical structure forming a lattice, the interaction of particles with a crystal may be different w.r.t. an amorphous medium.

Indeed, particle interaction with atoms of a crystal may occur through two routes: either with individual atoms as for an amorphous medium (incoherent scattering) or with an ordered ensemble of atoms in a crystal as a whole such as atomic strings or planes (coherent scattering). In the latter case, the interaction potentials of individual atoms have to be replaced with the collective potential of atomic strings or planes. Coherent interaction is observed when some conditions for alignment of the particle momentum with the crystal are met, while incoherent interaction is inherently isotropic.

Indeed this is well known in the Diffraction Theory. Diffraction occurs when the particle energy is sufficiently low, and therefore the De Broglie wavelength,

^ae-mail: sytov@fe.infn.it

λ , is comparable with the lattice spacing d_{at} . Diffraction is usually interpreted in terms of interference patterns in the elastic scattering cross section (coherent interaction), describing the interaction between radiation and the crystal lattice as a whole, i.e. scattering on different atoms cannot be considered independently [6]. For instance, diffraction of relatively low energy (10 eV–100 keV) electrons [7] interacting with crystalline solids proved to be a powerful tool to investigate the crystalline structure of matter.

At higher energies, λ becomes much shorter than d_{at} and one expects that coherent effects disappear. Nevertheless, at sufficiently high-energy, even if $\lambda \ll d_{at}$, the typical length of scattering region increases with the energy, being longer than d_{at} . Indeed, the length of the scattering region increases with the particle energy, E , embracing more and more atoms along a lattice direction. As for diffraction, the scattering by different atoms is also not independent in this case, and one has to consider the scattering of the particle by the crystal as a whole (coherent scattering). Naturally, coherent interaction adds up with incoherent scattering by individual atoms.

The first who understood the importance of the lattice structure in the interaction of high-energy particles with crystals were Ferretti and Ter-Mikaelyan, who exploited the Laue theory of diffraction to describe the interference effect of bremsstrahlung in crystals, so-called *coherent bremsstrahlung* (CB). CB is worldwide exploited at accelerator facilities [8,9,10], typically used in hadronic physics [11,12]. This phenomenon occurs even when the electron and positron incidence angles w.r.t. crystal planes and axes are small (less than 1°). At very small incidence angle, i.e. lower than the critical one introduced by Lindhard [13], a charged particle can be captured in the axial/planar potential well, i.e. *Channeling* occurs [14,15,16]. For particles moving in a crystal under channeling regime, the multiple scattering encountered is significantly different than if the particle would traverse an amorphous medium with the same density.

As described above, the scattering between the charged particle and crystal can be divided into coherent and incoherent parts. One may expect that in the case of absence of coherent scattering, the total multiple scattering is decreased with respect to an amorphous matter.

In this paper we introduce the effect of complete coherent scattering suppression (CSS) at certain crystal orientations, which we calculate under proper approximation. We report direct observation of CSS effect, determine the necessary conditions for its manifestation and model it via Monte Carlo simulations. More-

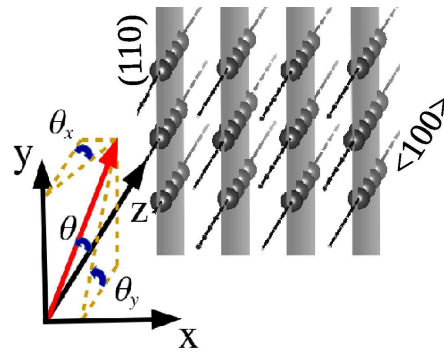


Fig. 1 Coordinate system to describe particle incidence on both the $\langle 100 \rangle$ atomic string and the (110) plane in a Si crystal.

over, we provide an evidence of partial CSS occurring at much broader incidence angle than the critical angle for channeling.

2 Basics of multiple scattering in a crystal

As for any situation when coherent and incoherent effects compete, the well known treatment borrowed from X-ray diffraction can be called forward and adapted to our circumstances. We adopted the work that Ter-Mikaelyan carried on for the case of bremsstrahlung [9] to the case of multiple scattering of charged particles in crystals. We introduced a theoretical calculation to explain CSS following a typical approach for X-ray diffraction [6], being applicable also for classical particle scattering by atomic strings and planes [18,17]. The particle-crystal interaction potential is described as the sum of individual particle-atom interaction potentials $U(\mathbf{r}) = \sum_j V(|\mathbf{r} - \mathbf{r}_j|)$, \mathbf{r} being the particle position and \mathbf{r}_j j -th atom location in the lattice. The latter differs from the equilibrium atomic position \mathbf{r}_{j0} due to thermal vibrations, $\mathbf{r}_j = \mathbf{r}_{j0} + \mathbf{u}_j$, \mathbf{u}_j being the uncorrelated displacement from the lattice nodes, characterized by the r.m.s. amplitude $\langle \mathbf{u}_j^2 \rangle$.

As a high-energy particle impinges on a crystal axis or plane at large enough angle, its wave function resembles a plane wave. Therefore, the Born approximation is traditionally applied to treat its interaction with the crystal by using the differential scattering cross-section ($\hbar = c = 1$):

$$\frac{d\sigma}{d\Omega} = \left| \sum_{j=1}^N e^{i\mathbf{q}\mathbf{r}_j} \right|^2 \frac{d\sigma_{at}}{d\Omega}, \quad (1)$$

where $\mathbf{q} = \mathbf{p} - \mathbf{p}'$ is the momentum transferred to the crystal lattice, N is the number of scattering centers in a crystal and $d\sigma_{at}$ the cross-section of scattering on a single atom. Hereinafter we will use the Coulomb screened

(Yukawa) atomic potential [2, 4], to calculate this cross-section. By assuming that atoms vibrate independently across their equilibrium positions, the total differential cross section (1) can be split into two parts [9, 6]

$$\frac{d\sigma}{d\Omega} = \frac{d\sigma_{coh}}{d\Omega} + \frac{d\sigma_{inc}}{d\Omega}, \quad (2)$$

where

$$\frac{d\sigma_{coh}}{d\Omega} = D \left| \sum_{j=1}^N e^{i\mathbf{q}\cdot\mathbf{r}_{j0}} \right|^2 \frac{d\sigma_{at}}{d\Omega} \quad (3)$$

is the "coherent" term of the differential cross section [9, 6] with the same form as the Laue-Bragg formula. This term represents the scattering process without any energy transfer to the crystal lattice, the probability of which is given by the Debye-Waller factor $D = \exp(-q^2 u_1^2)$, where u_1 is the one-dimensional amplitude of thermal oscillations $u_1^2 = \langle \mathbf{u}_j^2 \rangle / 3$. In turn, the "incoherent" term of the scattering cross section

$$\frac{d\sigma_{inc}}{d\Omega} = N(1 - D) \frac{d\sigma_{at}}{d\Omega} = \frac{d\sigma_{am}}{d\Omega} - \frac{d\sigma_1}{d\Omega} \quad (4)$$

is proportional to the probability $1 - D$, that an energy transfer occurs, and can be naturally separated into two contributions

$$\frac{d\sigma_{am}}{d\Omega} = N \frac{d\sigma_{at}}{d\Omega} \quad \text{and} \quad \frac{d\sigma_1}{d\Omega} = ND \frac{d\sigma_{at}}{d\Omega}, \quad (5)$$

where $d\sigma_{am}/d\Omega$ represents the scattering in an amorphous media, $d\sigma_1/d\Omega$ the difference between amorphous and crystal cases in differential cross-section of incoherent scattering unaccompanied by the atom vibration state change.

As the atom positions \mathbf{r}_{j0} are uncorrelated as in an amorphous medium, the cross section (3) exactly compensates for $d\sigma_1/d\Omega$ (5), making the total particle scattering cross section (2) both equal to $d\sigma_{am}/d\Omega$ (5) and independent of D . However, $d\sigma_{coh}/d\Omega$ (3) does not necessarily compensate for $d\sigma_1/d\Omega$ (5) in crystals. Indeed, at certain particle incidence direction, $d\sigma_{coh}/d\Omega$ can be practically nullified, manifesting thus the *coherent scattering suppression* (CSS) effect:

$$d\sigma \xrightarrow{d\sigma_{coh}=0} d\sigma_{am} - d\sigma_1. \quad (6)$$

In the case of a Si crystal oriented as in Fig. 1, the conditions in Eq. (6) for observation of the CSS effect, are naturally about the angles of incidence w.r.t. $\langle 100 \rangle$

axis, i.e. $\theta = \sqrt{\theta_x^2 + \theta_y^2} \approx \theta_y$ and (110) Si plane, i.e. θ_x . They should be chosen in the regions, respectively

$$\frac{10\theta_{ch}^{pl} d_{ax}}{\pi u_1} \approx 18 \text{ mrad} < \theta_y < \frac{\pi u_1}{d_{at}} \approx 43 \text{ mrad}, \quad (7)$$

where d_{at} is the interatomic distance in the $\langle 100 \rangle$ axis, and

$$10\theta_{ch}^{pl} \approx 2 \text{ mrad} < \theta_x < \frac{\pi u_1}{d_{ax}} \theta_y \approx 4.3 \text{ mrad}, \quad (8)$$

where d_{ax} is the interaxial distance for the (110) plane, θ_{ch}^{pl} for planar channeling critical angle. The left hand sides of both Eqs. (7) and (8) assure the necessary precision of straight line approximation [19]. Maximal CSS effect is attained at $\theta_y = 34.9 \text{ mrad}$ (2°) w.r.t. $\langle 100 \rangle$ Si axis and $\theta_x = 3 \text{ mrad}$ w.r.t. (110) Si plane. More information about this choice as well as about Born approximation theory on CSS effect is consider in appendix A.

3 Experimental results

Direct observation of CSS effect was carried out at the MAInz MIkrotron (MAMI) by scattering of 855 MeV electrons on either crystal or amorphous Si plate $l \sim 30 \mu\text{m}$ thick along the beam. The experimental setup is described in [20]. The crystalline plate was fabricated via anisotropic wet etching procedures [21], while the amorphous plate was produced by sputtering deposition of silicon onto a dedicated substrate, followed by anisotropic wet-chemical erosion to arrive at a thin amorphous plate surrounded by a bulky Si frame for mechanical stability [22]. Thickness was $34.2 \pm 0.2 \mu\text{m}$ for the crystal plate and $32.76 \pm 0.09 \mu\text{m}$ for the amorphous one. Following the method [23] with a high resolution x-ray diffractometer, we verified their structure and measured that the two plates differ in *mass* thickness by 0.4 % only. The angular distributions of horizontal scattering angles ϑ_x for both kinds of plates as well as the difference of these distributions are illustrated in Fig. 2.

Table 1 Molière theory parameters for silicon crystal ($\theta_x = 3 \text{ mrad}$, $\theta_y = 34.9 \text{ mrad}$ (2°)) and amorphous plates, calculated by (9-10) and by fitting both experimental and simulation data

ϑ (μrad)	experiment	simulation	Molière theory
ϑ_s^{cr}	183.4 ± 2.0	181.5 ± 0.6	178.6 ± 0.6
ϑ_s^{am}	196.5 ± 2.0	197.3 ± 0.3	195.6 ± 0.3
ϑ_{min}^{cr}	17.3 ± 0.8	18.0 ± 0.4	19.25
ϑ_{min}^{am}	12.5 ± 0.7	12.30 ± 0.13	12.83

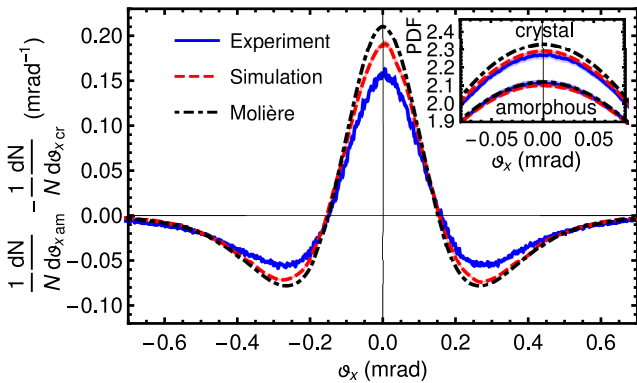


Fig. 2 The difference of the angular distributions of deflected beam by a silicon crystal, aligned at $\theta_x = 3 \text{ mrad}$, $\theta_y = 34.9 \text{ mrad}$ (2°) and amorphous membranes for experiment (solid), simulations (dashed) and Molière model (dot dashed). The distributions themselves are placed in insert. The curve width represents the errors.

We used Molière theory [2,3] to calculate the distribution of horizontal scattering angles ϑ_x

$$p(\vartheta_x) = \frac{1}{\pi} \int_{-\infty}^{\infty} \sum_{j=0}^{\infty} \left(\frac{\vartheta_s}{\vartheta_c}\right)^{2j} f^{(j)} \left(\sqrt{\frac{\vartheta_x^2 + \vartheta_y^2}{2\vartheta_s^2}}\right) d\vartheta_y, \quad (9)$$

$$\vartheta_c = \alpha[Z(Z+1)z4\pi n_{at}l]^{1/2}/pv,$$

where p and v are the particle momentum and velocity respectively, α the fine structure constant, n_{at} the atomic density, Z the atomic number, z the particle charge in e units, the functions $f^{(j)}$ are introduced in [2,3].

ϑ_s is the only free parameter of Molière theory, which is of the order of the r.m.s. of distribution $p(\vartheta_x)$. Indeed, at lowest order ($j = 0$), ϑ_s is exactly the r.m.s. of the distribution. For comparison with the experimental results, $p(\vartheta_x)$ was convoluted with the angular distribution of the beam characterized by $27 \mu\text{rad}$ divergence. In Table 1 ϑ_s is reported for 3 different cases: by fitting of experimental data with Eq. (9), by fitting in the same way of the distributions obtained by Monte Carlo simulations described below and by a full theoretical estimation also described below. The difference between ϑ_s for the crystalline and amorphous cases are reported for all these 3 cases in Fig. 2 and showing a firm observation of the CSS.

According to Molière theory [2,3], the theoretical value ϑ_s is defined as a function of an effective minimal scattering angle $\vartheta_{min}^{am} = \hbar/Rp$, evaluated through the Coulomb screened (Yukawa) atomic potential, where $R = a_{TF}(1.13 + 3.76(\alpha Zz/\beta)^2)^{-1/2}$ is the atom screening radius, chosen according to [2,3], $a_{TF} = 0.8853a_B Z^{-1/3}$ the Thomas-Fermi screening radius, a_B the Bohr radius. The CSS effect in crystals can be similarly de-

scribed by introducing the effective minimal scattering angle ϑ_{min}^{cr} , obeying the relation

$$\ln \vartheta_{min}^{cr} = \ln \vartheta_{min}^{am} + \frac{0.5Z}{Z+1} \left[\left(1 + \frac{u_1^2}{R^2}\right) e^{\frac{u_1^2}{R^2}} E_1\left(\frac{u_1^2}{R^2}\right) - 1 \right], \quad (10)$$

obtained by integration of the cross section (4) following the Molière theory [2,3] at the condition of complete coherent scattering suppression $d\sigma_{coh}/d\Omega = 0$. E_1 is the exponential integral. The last item in (10) is representation of the $d\sigma_1/d\Omega$ contribution in (4), manifesting the difference in incoherent scattering between the crystalline and amorphous cases. The ratio $Z/(Z+1)$ is necessary to exclude from the CSS effect scattering on atomic electrons, described by “+1” in the definition of ϑ_c (see Eq. (9)) [3].

According to Eq. (10), the CSS effect can be interpreted as the increase in the effective minimal scattering angle from ϑ_{min}^{am} to ϑ_{min}^{cr} . Both of these values as well as the corresponding angles ϑ_s are summarized in Table 1 and used for calculation of the theoretical angular distributions (Molière theory) by Eq. (9) as shown in Fig. 2. The experimental and simulated values for ϑ_{min}^{am} and ϑ_{min}^{cr} shown in Table 1 were calculated from the corresponding values ϑ_s in Table 1.

Both the experiment and the theory demonstrate the extent of CSS effect although the agreement is not perfect. However, neither Born approximation nor Molière theory, modified using Eq. (10), take into consideration the residual coherent effects, such as the influence of the string potential on incoherent scattering and an additional angular spread arising at both the entrance and exit of a particle in/out of a crystal. All these effects have been fully taken into consideration by using the CRYSTAL code [24,25], a program for Monte Carlo simulations of charged particle trajectories in the potential of a crystalline medium with simulation of incoherent scattering, tested in different experiments [26, 27,28]. The results of simulations are shown in Fig. 2 and Table 1.

The CSS effect was also investigated both experimentally and by simulations over a wide range of particle incidence directions θ_y and θ_x including the values beyond the optimal angular range of Eqs. (7-8).

The corresponding angular distributions were used for a fit of Molière theory to calculate dependence of ϑ_s on both θ_y and θ_x , as shown in Figs. 3a and 3b, respectively. The horizontal lines indicate the ϑ_s values evaluated for the amorphous case using Molière theory. The values of θ_y and θ_x used in Fig. 3a and 3b are shown in Fig. 3c.

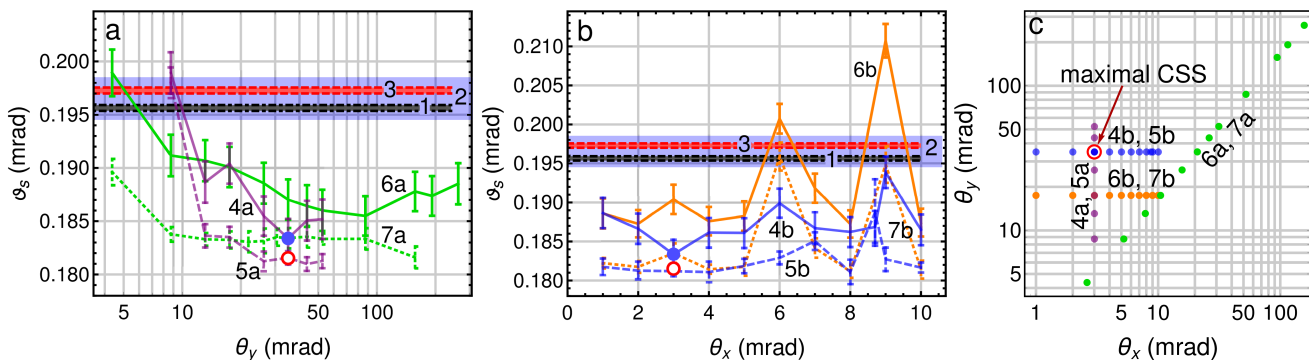


Fig. 3 Dependence of angle ϑ_s on the vertical (a) and horizontal (b) angles of crystal orientation. The lines 1–3 are the results for the amorphous target by the Molière model, experiment and simulations, respectively. Curve pairs (4,5), (6,7) represent the results for the crystal target. Even numbers are for experiment (solid curves), odd numbers are for CRYSTAL simulations (dashed curves). a: (4a, 5a) θ_x is fixed at 3 *mrad*; (6a, 7a) both θ_x and θ_y are varied while keeping the ratio $\theta_x/\theta_y = 0.6$ constant to avoid the intersection with high miller index crystalline planes. b: θ_y is fixed (4b, 5b) at 34.9 *mrad* (2°); (6b, 7b) to 17.5 *mrad* (1°). Blue disks (experiment) and red circles (CRYSTAL simulations) are the results for crystal alignment for maximal CSS effect $\theta_x = 3$ *mrad*, $\theta_y = 34.9$ *mrad* highlighted in Fig. 2 and Table 1. The errors are given by the thickness of the lines for the amorphous target as well as by the error bars for the crystal. c: the values of angles θ_x and θ_y , used in corresponding curves in (a) and (b).

Fig. 3a demonstrates that although the full CSS effect is attained within a relatively narrow angular region as in Eqs. (7–8), a considerable partial CSS is still observed at least up to $\theta_x \sim 157$ *mrad* (9°), $\theta_y \sim 262$ *mrad* (15°) (see Fig. 3a). Since the other axes can contribute at such high angular values, some partial CSS effect can appear at any crystal alignment.

Fig. 3b reveals that the CSS effect may be hampered at relatively large incidence angles by the appearance of the peaks originating from the coherent scattering on high-index planes, which were observed experimentally as well as predicted by simulations especially in scan 6b at 6 and 9 *mrad* of θ_x .

Thereby, we conclude that the anisotropy of multiple scattering can be observed at broad angle w.r.t. the crystalline orientations. Furthermore, at higher energies the CSS effect is preserved, since neither the right hand side of Eq. (10) nor the upper angular limits in (7–8) depend on energy for ultrarelativistic particles, while the lower limits decrease further with energy. By the same reason the anisotropy of multiple scattering of ultrarelativistic particles depends neither on the particle mass nor on its charge sign. However, the effect is attenuated as the particle charge rises, becoming negligible for high- z ions.

4 Conclusions

In conclusion, the maximal effect of CSS in crystals has been observed under proper choice of the incidence angle. It resulted in decrease by about 7 % in the multiple scattering angle in a thin Si crystal target with the same mass thickness as an amorphous one.

Partial CSS does exist and was observed even up to about 15° tilt from the crystal axis, owing to its independence on energy, mass and charge sign. We believe that the angular dependence of multiple scattering may be useful knowledge to aid the modeling and design of nuclear physics and high-energy experiments. For instance, Geant4 [4], currently using the Molière model of scattering [2,3], may be implemented with the model developed in this work.

Acknowledgements We acknowledge partial support of the INFN-ELIOT experiment and by the European Commission (the PEARL Project within the H2020-MSCA-RISE-2015 call, GA 690991). E. Bagli, L. Bandiera and A. Mazzolari recognize the partial support of FP7-IDEAS-ERC CRYSBREAM project GA n. 615089. A. Mazzolari and V. Guidi acknowledge founding from PRIN 2015LYYXA8 “Multi-scale mechanical models for the design and optimization of microstructured smart materials and metamaterials”. We also acknowledge the CINECA award under the ISCRA initiative for the availability of high performance computing resources and support. We acknowledge Professor H. Backe for fruitful discussions.

Appendix A: Theory of multiple scattering in a crystal

In this appendix we apply Born approximation [6,9,18] to establish the conditions, in particular for crystal alignment, for coherent scattering suppression in a crystal owing to by the discreteness of momentum transfer, in particular Eqs. (7) and (8) in the main text. Calculation was done in the case of $\langle 100 \rangle$ axis and (110) plane of a Si crystal.

In order to find the conditions for coherent scattering suppression, one should compare the r.m.s. angle $\langle \vartheta_{x'}^2 \rangle_{coh}^1$ of coherent scattering with the r.m.s. angle $\langle \vartheta_1^2 \rangle$, characterizing the suppression of incoherent scattering, established by the cross-sections defined in the paper as $d\sigma_{coh}$ and $d\sigma_1$, respectively. In other words, the difference of the total r.m.s. scattering angle in amorphous matter and in a crystal is $\langle \vartheta_{x'}^2 \rangle_{coh} - \langle \vartheta_1^2 \rangle$. The condition for complete coherent scattering suppression holds

$$\langle \vartheta_{x'}^2 \rangle_{coh} / \langle \vartheta_1^2 \rangle \ll 1. \quad (\text{A.1})$$

$\langle \vartheta_1^2 \rangle$ is obtained by integration of the cross-section $d\sigma_1$ as follows

$$\langle \vartheta_{x'}^2 \rangle_1 = n_{at} l \int \vartheta_{x'}^2 \frac{d\sigma_1}{d\Omega} d\Omega = n_{at} l \int \frac{q_{x'}^2}{p^2} \frac{d\sigma_1}{d\Omega} d\Omega = \frac{\theta_1^2}{2} \left[\left(1 + \frac{u_1^2}{R^2} \right) e^{\frac{u_1^2}{R^2}} E_1 \left(\frac{u_1^2}{R^2} \right) - 1 \right] \quad (\text{A.2})$$

see definitions of such quantities in the paper.

Similarly, one can calculate the angle $\langle \vartheta_{x',y'}^2 \rangle_{coh}$ by using the cross-section $d\sigma_{coh}$. With this aim, one can express a direct summation of the exponents over the $8N^3$ atoms of N^3 elementary cells as

$$\left| \sum_{j=1}^{8N^3} e^{i\mathbf{q}\cdot\mathbf{r}_{j0}} \right|^2 = \left(\frac{2\pi N}{d_{at}} \right)^3 \sum_{n_1=-\infty}^{\infty} \sum_{n_2=-\infty}^{\infty} \sum_{n_3=-\infty}^{\infty} |S|^2 \times \delta \left(q_1 - \frac{2\pi n_1}{d} \right) \delta \left(q_2 - \frac{2\pi n_2}{d} \right) \delta \left(q_3 - \frac{2\pi n_3}{d} \right) \quad (\text{A.3})$$

where d_{at} is lattice spacing and S the structure factor, which can be written for diamond-type crystal lattice [9, 18] as

$$S = \left[1 + e^{i\pi(n_1+n_2+n_3)/2} \right] [1 + \cos(\pi(n_1+n_2)) + \cos(\pi(n_2+n_3)) + \cos(\pi(n_1+n_3))] \quad (\text{A.4})$$

1, 2 and 3 correspond to the Cartesian axes associated with the canonical base. In addition, one should [6] average the cross section $d\sigma_{coh}/d\Omega$ over initial beam angular distribution. For certain cylindrical Gaussian, the following angular distribution will be used

$$\frac{1}{N} \frac{dN}{d\vec{\theta}} = \frac{1}{2\pi\delta^2} e^{-\left(\vec{\theta}-\vec{\theta}_0\right)^2/2\delta^2}, \quad (\text{A.5})$$

where $\vec{\theta} = (\vec{\theta}_1, \vec{\theta}_2)$ are the angles of integration, $\vec{\theta}_0 = (\vec{\theta}_{01}, \vec{\theta}_{02})$ the mean angles of beam direction w.r.t. the crystal planes 23 and 13 respectively. Thereby, θ_0 is the

¹ $x'y'z'$ is the Cartesian coordinate system connected with an incident particle, the momentum \vec{p} of which is parallel to z'

beam angle w.r.t. the axis 3. Both angles are hereinafter considered as small angles: $\theta \ll 1$, $\theta_0 \ll 1$. δ is the r.m.s. angular divergence. The actual value of δ can vary in the range of $\sim 20 - 200 \mu\text{rad}$ through the passage of a $\sim 30 \mu\text{m}$ Si target. Since the typical incidence angles well exceed $1 \text{ mrad} \gg \delta$, the beam angular divergence can be treated as negligible and assumed to be independent on particle penetration depth.

By substituting $d\sigma_{coh}$ for $d\sigma_1$ in (A.2) and by using (A.3), (A.4), (A.5) one finally obtains

$$\left\{ \langle \vartheta_{x'}^2 \rangle_{coh} \right\} = \int \left\{ \vartheta_{x'}^2 \right\} \frac{d\sigma_{coh}}{d\Omega} d\Omega = \frac{1}{p^2} \int \left\{ \frac{q_{x'}^2}{q_{y'}^2} \right\} \frac{d\sigma_{coh}}{d\Omega} d\Omega = \left(\frac{2\alpha Z}{\theta_0 p v} \right)^2 \left(\frac{2\pi}{d_{at}} \right)^3 \frac{n_{at} l}{8} \sum_{n_1=-\infty}^{\infty} \sum_{n_2=-\infty}^{\infty} \sum_{n_3=-\infty}^{\infty} |S|^2 \times \left\{ \frac{(\theta_{01} q_{2n_2} - \theta_{02} q_{1n_1})^2}{q_{3n_3}^2} \right\} \frac{q_{n_1 n_2}}{q_{n_1 n_2 n_3}} \frac{\exp(-q_{n_1 n_2 n_3}^2 u_1^2)}{(q_{n_1 n_2 n_3}^2 + R^{-2})^2} \times \frac{1}{\sqrt{2\pi\delta q_{n_1 n_2 n_3}}} \exp[-(q_{3n_3} + q_{1n_1}\theta_{01} + q_{2n_2}\theta_{02})^2/2\delta^2 q_{n_1 n_2}^2], \quad (\text{A.6})$$

where $q_{n_1 n_2}^2 = q_{1n_1}^2 + q_{2n_2}^2$ and $q_{n_1 n_2 n_3}^2 = q_{n_1 n_2}^2 + q_{3n_3}^2$. It is important to underline, that Eq. (A.6) is valued for any type of a crystal lattice as well as for any axes. Then, the structure factor is set as well as the directions of 1,2,3 are assigned for the particular case under investigation. To simplify the integration of (A.6) on angles $d\theta_1 d\theta_2$, these angles were transformed by rotation of the coordinate system around axis 3 by angle φ , for which $\cos \varphi = q_{1n_1}/q_{n_1 n_2}$, $\sin \varphi = q_{2n_2}/q_{n_1 n_2}$, and in which the second component of q is equal to 0. We also applied the momentum conservation law $q_{1n_1}\theta_{01} + q_{2n_2}\theta_{02} = q_{n_1 n_2}\theta \cos \varphi = -q_{3n_3} \cos \theta$ ($p'^2 = (\vec{p}' + \vec{q})^2 = p^2$).

Here φ is the angle formed by the transferred momentum projection onto the plane $12 \vec{q}_{n_1 n_2}$ and the vector $\vec{\theta}$. One can pass to the same law in the negligible divergence limit $\delta \rightarrow 0$, arriving to the condition

$$q_{n_1 n_2 n_3}^2 = q_{3n_3}^2 (1 + \cos^2 \varphi / \theta^2) > q_{3n_3}^2 / \theta^2, \quad (\text{A.7})$$

which limits the momentum transfer value from below at $q_{n_3} \neq 0$. By rewriting Eq. (A.7) in terms of the Debye-Waller factor, which presents in (A.6)

$$D = \exp(-u_1^2 q^2) \leq \exp(-u_1^2 q_{3n_3}^2 / \theta^2), \quad (\text{A.8})$$

we conclude that the discrete nature of the longitudinal momentum transfer $q_{n_3} = 2\pi n_3 / d_{at}$ results in coherent scattering suppression by the Debye-Waller factor at $q > \hbar / u_1$. By assuming that $D \leq 0.01$, and substituting the minimal momentum axial transfer value $q_{31} = 2\pi / d_{at}$, one readily comes to the first condition for coherent scattering suppression

$$\theta < \frac{u_1 q_{31}}{2} = \frac{\pi u_1}{d_{at}} \approx 43 \text{ mrad} (2.5^\circ). \quad (\text{A.9})$$

This condition represents *coherent scattering suppression by individual atoms in the strings*, when separate atomic strings scatter charged particles as a whole. The suppression range (A.9) is illustrated in Fig. 4a, representing the ratio $\langle \vartheta_{x'}^2 \rangle_{coh} / \langle \vartheta_1^2 \rangle$.

If the condition (A.9) is fulfilled, one can neglect the component q_{3n3} in (A.6). By assigning the coordinate system 1,2,3 to the system x, y, z , in which z is parallel to $\langle 100 \rangle$ Si axes as well as the planes (-110) and (110) are formed by xz and yz planes, respectively, and by using the structure factor (4A), one can rewrite (6A) as

$$\langle \vartheta_{x'}^2 \rangle_{coh} = \int \vartheta_{x'}^2 \frac{d\sigma_{coh}}{d\Omega} d\Omega = \frac{1}{p^2} \int q_{x'}^2 \frac{d\sigma_{coh}}{d\Omega} d\Omega = \left(\frac{2\alpha Z}{\theta_0 p v} \right)^2 \frac{2\pi}{d_{at}} \frac{2\pi}{d_{ax}} \frac{2\pi}{d_{pl}} n_{at} l \times \sum_{m=-\infty}^{\infty} \sum_{k=-\infty}^{\infty} (\theta_{0x} q_{ym} - \theta_{0y} q_{xk})^2 \frac{\exp(-q_{mk}^2 u_1^2)}{(q_{mk}^2 + R^{-2})^2} \times \frac{1}{\sqrt{2\pi\delta q_{mk}}} \exp[-(q_{xk}\theta_{0x} + q_{ym}\theta_{0y})^2 / 2\delta^2 q_{mk}^2], \quad (\text{A.10})$$

where $q_{mk}^2 = q_{xk}^2 + q_{ym}^2$, $d_{pl} = d_{ax} = d' = d_{at}/2\sqrt{2}$, $q_{xk} = 2\pi k/d_{pl}$ and $q_{ym} = 2\pi m/d_{ax}$, $k, m = 0, \pm 1, \pm 2, \dots$. Here the structure factor is trivial, i.e. $|S|^2 = 1$. Eq. (A.10) represents the case $q_z = 0$, defined by the condition (A.9). This equation was used for calculation of the dependence of the average squared angle $\langle \vartheta_{x'}^2 \rangle_{coh} / \langle \vartheta_1^2 \rangle$ on θ_y in the limit $q_z = 0$.

The momentum conservation law can be obtained similarly by Eq. (A.7) under the limit of negligible divergence $\delta \rightarrow 0$, $q_{xn} = -q_{ym}\theta_y/\theta_x$, $q_{mk}^2 = q_{xk}^2 + q_{ym}^2 = q_{ym}^2 \theta^2 / \theta_x^2$, giving the condition for the Debye-Waller factor (compare (A.8)):

$$D = \exp(-u_1^2 q^2) = \exp[-u_1^2 (q_x^2 + q_y^2)] \leq \exp(-u_1^2 q_1^2 \theta^2 / \theta_x^2). \quad (\text{A.11})$$

Assuming again $D \leq 0.01$ one arrives to the second condition for coherent scattering suppression:

$$10\theta_{ch}^{pl} \approx 2 \text{ mrad} < \theta_x < u_1 q_{y1} \theta_y / 2 = \frac{\pi u_1}{d_{ax}} \theta_y \approx 0.12\theta_y \approx 4.3 \text{ mrad}. \quad (\text{A.12})$$

This condition represents *coherent scattering suppression by individual strings in the planes*, when separate planes scatter charged particles as a whole. $q_{y1} = 2\pi/d_{ax} = 4\sqrt{2}\pi/d_{at}$ is the minimal momentum transfer parallel to the yz or (110) plane. The numerical estimate (A.12) has been done for the chosen axial angle $\theta = 2^\circ$. The suppression range (A.12) is illustrated in Fig. 4b, representing the ratio $\langle \vartheta_{x'}^2 \rangle_{coh} / \langle \vartheta_1^2 \rangle$ in dependence on the horizontal angle θ_x . The peaks in this dependence originate from the coherent scattering on high-index planes. One can eliminate their influence by the application of the limit isolated plane ($d_{pl} \rightarrow \infty$).

Following condition (A.11) one can rewrite Eq. (A.10) as

$$\langle \vartheta_{x'}^2 \rangle_{coh} = \left(\frac{2\alpha Z}{\theta_0 p v} \right)^2 \frac{2\pi}{d_{at}} \frac{2\pi}{d_{ax}} n_{at} l \frac{\theta_x^2 + \theta_y^2}{\theta_x^3} \times \sum_{m=-\infty}^{\infty} q_{ym}^2 \frac{\exp(-u_1^2 q_{ym}^2 (\theta_x^2 + \theta_y^2) / \theta_x^2)}{(q_{ym}^2 (\theta_x^2 + \theta_y^2) / \theta_x^2 + R^{-2})^2}. \quad (\text{A.13})$$

This equation was used to build up the dependence illustrated in Fig. 4b in the limit of isolated plane, eliminating the contribution by high-index planes, but preserving the range of coherent scattering suppression, defined by the condition (A.12).

The left hand side condition (A.12), in which θ_{ch}^{pl} is the planar channeling angle, has been implied to assure sufficient precision of Born approximation. It follows, directly from the estimate of the influence of particle deflection in the average planar potential on the angle of incoherent electron scattering by nuclei [19], which cannot be estimated in Born approximation. The condition (A.12) can be substituted in (A.9)

$$\frac{10\theta_{ch}^{pl} d_{ax}}{\pi u_1} \approx 18 \text{ mrad} (1^\circ) < \theta_y \leq \theta < \frac{u_1 q_{31}}{2} = \frac{\pi u_1}{d_{at}} \approx 43 \text{ mrad} (2.5^\circ). \quad (\text{A.14})$$

Fig. 4c illustrates the region of practically complete suppression $\langle \vartheta_{x'}^2 \rangle_{coh} < 0.01 \langle \vartheta_1^2 \rangle$ (as required by (A.1)) of the coherent scattering (central dark triangle) predicted by Eqs. (A.12) and (A.14). This coordinate point $\theta_x = 3 \text{ mrad}$ and $\theta_y = 2^\circ \approx 35 \text{ mrad}$, marked by the white cross, corresponds to the electron incidence direction, which has been selected as the most appropriate one for the conducted experiment on the first observation of the coherent scattering suppression effect, presented in Fig. 2 of the paper.

References

1. M. Tanabashi et al. (Particle Data Group), Review of Particle Physics, Phys. Rev. D **98**, 030001 (2018).
2. G. Molière, Z. Naturforsch. **3a**, 78-97 (1948).
3. H. Bethe, Phys. Rev. **89**, 1256-1266 (1953).
4. GEANT4 4 10.5 Physics Reference Manual, <http://geant4.cern.ch/>.
5. T.T. Böhlen et al. The FLUKA Code: Developments and Challenges for High Energy and Medical Applications, Nuclear Data Sheets **120**, 211-214 (2014)
6. L. Landau, L. Pitaevskii, E. Lifshitz. Electrodynamics of Continuous Media. Vol. 8 (2nd ed.) (Butterworth-Heinemann, 1984), ISBN-10: 0750626348.
7. R. W. James, The optical principles of the diffraction of x-rays. (G. Bell And Sons Limited, 1962).
8. B. Ferretti, Nuovo Cimento **7**, 118 (1950).
9. M. L. Ter-Mikaelian, High-Energy Electromagnetic Processes in Condensed Media (Wiley, New York, 1972).

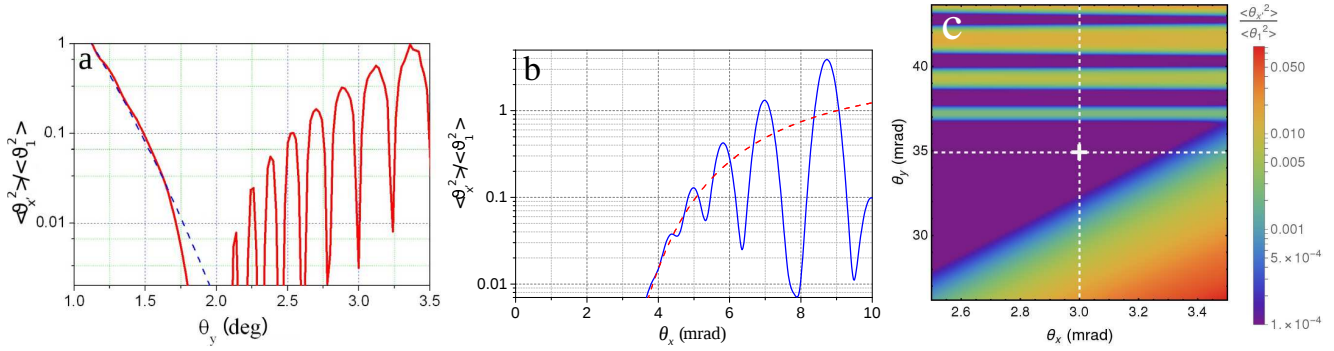


Fig. 4 “Planar” and “axial” dependence of the average squared angle $\langle \vartheta_{x'}^2 \rangle_{coh} / \langle \vartheta_1^2 \rangle$ (calculated with Eqs. (A.6) and (A.2)) of coherent 855 MeV electrons scattering by (110) planes in a 30 μm Si crystal on both incidence angles, θ_x and θ_y respectively. (a): “Axial” dependence, evaluated at $\theta_x = 3$ mrad with both $q_z = 0$ and all the $q_z \neq 0$ contributions (red solid line), the left dashed blue line is the $q_z = 0$ contribution (A.10). (b) “Planar” dependence, evaluated at $\theta_y = 34.9$ mrad (2°) with both $q_z = 0$ and all the $q_z \neq 0$ contributions (blue solid line), while the red dashed line was evaluated in the limit of isolated plane (A.13). (c): The same dependence on both θ_x and θ_y angles. White cross marks the optimal orientation for coherent scattering suppression $\theta_x = 3$ mrad and $\theta_y = 34.9$ mrad, dashed horizontal and vertical lines represent solid curves on plots (a) and (b) respectively.

10. H. Überall, High-energy interference effect of bremsstrahlung and pair production in crystals, *Phys. Rev.* **103**, 1055 (1956).
11. D. Lohmann, et al., *Nucl. Instrum. Methods Phys. Res. A* **343**, Issues 2-3, 494 (1994).
12. C. A. Paterson et al. (CLAS Collaboration), *Phys. Rev. C* **93**, 065201 (2016).
13. J. Lindhard, *Kgl. Dan. Vid. Selsk. Mat.-Fys. Medd.* **34** No 4, 2821–2836 (1965).
14. J. Stark, *Zs. Phys.* **13**, 973–977 (1912).
15. J. A. Davies, J. Friesen, J. D. McIntyre, *Can J. Chem.* **38**, 1526–1534 (1960).
16. M. T. Robinson, O. S. Oen, *Appl. Phys. Lett.* **2**, 30–32 (1963).
17. A. I. Akhiezer, N. F. Shul’ga, *High Energy Electrodynamics in Matter.* (Gordon and Breach, New York, 1996), ISBN 2-88449-014-0.
18. V. N. Baier, V.M. Katkov, and V.M. Strakhovenko, *Electromagnetic Processes at High Energies in Oriented Single Crystals* (World Scientific, Singapore, 1998).
19. V. A. Bazylev, V. V. Goloviznin, A. V. Dernura, *Zh. Eksp. Teor. Fiz.* **92**, 1946-1958 (1987).
20. D. Lietti et al., *Review of Scientific Instruments* **86**, 045102 (2015).
21. W. Scandale et al., *Phys. Lett. B* **734**, 1-6 (2014).
22. Y. P. Xu, R. S. Huang, G. A. Rigby, *J. of Electr. Mat.* **21**, Issue 3, 373-381 (1992).
23. D. C. Creagh and J. H. Hubbell, *Acta Cryst. A* **43**, 102-112 (1987).
24. A. I. Sytov, *Vestnik BSU (in russian)*, Series **1** N2, 48-52 (2014).
25. A. I. Sytov, V. V. Tikhomirov, *Nucl. Instr. and Meth. in Phys. Res. B* **355**, 383-386 (2015).
26. A. Mazzolari et al., *Phys. Rev. Lett.* **112**, 135503 (2014).
27. L. Bandiera et al. *Phys. Rev. Lett.* **115**, 025504 (2015).
28. V. Guidi, L. Bandiera, V.V. Tikhomirov, *Phys. Rev. A* **86**, 042903 (2012).